Dear author,

Please note that changes made in the online proofing system will be added to the article before publication but are not reflected in this PDF.

We also ask that this file not be used for submitting corrections.

International Journal of Radiation Oncology biology • physics

www.redjournal.org

Clinical Investigation

Establishment of Microbeam Radiation Therapy at a Small-Animal Irradiator

Franziska Treibel,*,†,‡ Mai Nguyen,*,† Mabroor Ahmed,*,†,‡ Annique Dombrowsky,*,† Jan J. Wilkens,*,‡ Stephanie E. Combs,*,† Thomas E. Schmid,*,† and Stefan Bartzsch*,†

*School of Medicine, Klinikum rechts der Isar, Department of Radiation Oncology, Technical University of Munich, Munich, Germany; †Institute for Radiation Medicine, Helmholtz Centre Munich, Munich, Germany; and ‡Physics Department, Technical University of Munich, Garching, Germany

Received Mar 24, 2020. Accepted for publication Sep 21, 2020.

Purpose: Microbeam radiation therapy is a preclinical concept in radiation oncology. It spares normal tissue more effectively than conventional radiation therapy at equal tumor control. The radiation field consists of peak regions with doses of several hundred gray, whereas doses between the peaks (valleys) are below the tissue tolerance level. Widths and distances of the beams are in the submillimeter range for microbeam radiation therapy. A similar alternative concept with beam widths and distances in the millimeter range is presented by minibeam radiation therapy. Although both methods were developed at large synchrotron facilities, compact alternative sources have been proposed recently.

Methods and Materials: A small-animal irradiator was fitted with a special 3-layered collimator that is used for preclinical research and produces microbeams of flexible width of up to 100 μm. Film dosimetry provided measurements of the dose distributions and was compared with Monte Carlo dose predictions. Moreover, the micronucleus assay in Chinese hamster CHO-K1 cells was used as a biological dosimeter. The focal spot size and beam emission angle of the x-ray tube were modified to optimize peak dose rate, peak-to-valley dose ratio (PVDR), beam shape, and field homogeneity. An equivalent collimator with slit widths of up to 500 μm produced minibeams and allowed for comparison of microbeam and minibeam field characteristics.

Results: The setup achieved peak entrance dose rates of 8 Gy/min and PVDRs >30 for microbeams. Agreement between Monte Carlo simulations and film dosimetry is generally better for larger beam widths; qualitative measurements validated Monte Carlo predicted results. A smaller focal spot enhances PVDRs and reduces beam penumbras but substantially reduces the dose rate. A reduction of the beam emission angle improves the PVDR, beam penumbras, and dose rate without impairing field homogeneity. Minibeams showed similar field characteristics compared with microbeams at the same ratio of beam width and distance but had better agreement with simulations.

Conclusion: The developed setup is already in use for in vitro experiments and soon for in vivo irradiations. Deviations between Monte Carlo simulations and film dosimetry are attributed to scattering at the collimator surface and manufacturing inaccuracies and are a matter of ongoing research.

Corresponding author: Stefan Bartzsch; E-mail: stefan.bartzsch@tum.de

This research was funded by the German Research Foundation, grant #389238549.

Disclosures: The authors reported no disclosures or conflicts of interest.

Research data are stored in an institutional repository and will be shared upon request to the corresponding author.

Int J Radiation Oncol Biol Phys, Vol. ■, No. ■, pp. 1–11, 2020
0360-3016/$ - see front matter
https://doi.org/10.1016/j.ijrobp.2020.09.039

Introduction

Microbeam radiation therapy (MRT) is a preclinical method in radiation oncology with the potential to substantially improve the therapeutic efficacy of radiation therapy without increasing side effects.[1] In MRT, a collimator spatially modulates the radiation dose on a micrometer scale, a concept that has been termed *spatial fractionation*.[2] Arrays of planar beams a few tens of micrometers wide are created, with unconventionally high peak doses of several hundred grays. These beams are separated by low dose regions (valleys) with doses below the tissue tolerance level. Such beam geometries spare normal tissue compared with conventional treatments,[3-6] and microbeams have successfully ablated tumors in mice and rats.[3,7-9] Although the radiobiological mechanisms are little understood, preclinical data suggest that the close vicinity of high and low dose values triggers an immune response.[10,11]

The application of MRT is technically challenging. Generation of beam profiles on a micrometer scale that maintain their shape with increasing depth in the patient demands low beam divergence, a small source size, and photon energies in the order of 100 keV. Short exposure times, and hence high dose rates, are required to avoid blurring of the micrometer-sized dose patterns owing to cardiovascular or respiratory motion in the tissue.[12,13] Until now, only large, third-generation synchrotrons have provided suitable beam properties, which has limited development of MRT in the past 25 years to a couple of large synchrotron facilities such as the European Synchrotron Radiation Facility in Grenoble, France.

Compact microbeam irradiators based on inverse Compton scattering,[14,15] carbon nanotube sources,[16] and converted x-ray tubes[17] have been suggested. However, so far, none of them have achieved the clinically required beam properties.

X-ray tubes, a cost-effective and easily handled source, have also been used for preclinical research with microbeams. Nevertheless, the low dose rate, the strongly divergent radiation field, and the large source size of conventional x-ray tubes are a challenge for experiments with microbeams. Most existing x-ray tube–based systems provide only larger beam widths greater than 100 μm,[18-20] which are typically referred to as minibeams, at dose rates less than 5 Gy/min. With carbon nanotube sources, MRT treatments of mice at low dose rates have successfully been carried out[21] and demonstrated that the effect of motion-induced dose blurring for microbeams can be limited by proper fixation of the animals during irradiation.

Bartzsch et al[22] demonstrated the generation of preclinical microbeams 50 μm in width for in vitro experiments with an x-ray tube. They used a tungsten collimator with a fixed slit width and tilted slits. By moving the collimator to a distance of only 7 cm from the focal spot and placing the sample directly in front of the collimator, they achieved high dose rates of up to 18 Gy/min. However, the large beam divergence, the field inhomogeneity, and a rapidly decreasing ratio between peak and valley doses with distance to the collimator render such a system unsuitable for in vivo treatments.

Recent technical developments in preclinical radiation therapy research strive to mimic clinical standards and improve comparability to clinical treatments. Small-animal irradiators have been developed that provide image guidance and adaptive treatment planning.[23] Prezado et al[20] and Esplen et al[24] developed minibeam setups for such systems. Prezado et al made major modifications to the small-animal platform by introducing multiple stages. Using a divergent slit collimator with a central slit width of 400 μm, they created 7 minibeams with peak dose rates of up to 3.5 Gy/min in a depth of 1 cm. Inhomogeneity across the radiation field was observed, and the peak dose rate decreased by 40% toward the outer beams. Esplen et al used a parallel multislit collimator built from steel bars separated by double-sided tape. For the small anode focal spot, they measured 0.5 Gy/min at a phantom surface at a collimator distance of 3 cm. Slit width varied largely around 155 μm, and the field uniformity suffered from the collimator's parallel slit orientation. Both setups produced minibeams, and to the knowledge of the authors, no such system in the microbeam domain exists with beam widths of less than 100 μm.

The current study presents a system capable of producing microbeams of variable beam width between a few tens of micrometers and 100 μm at dose rates of up to 8.0 Gy/min in a small-animal irradiator. A collimator with adjustable slit width and tilted slits was mounted at a source distance of 21.2 cm. The radiation geometry was modified by adjusting the beam emission angle, slit width, and focal spot, and the individual parameters were optimized with regard to dose rate, peak-to-valley dose ratio (PVDR), and field homogeneity. The relatively high dose rate and the homogeneous field facilitated preclinical in vivo studies with high peak doses under flexible field configurations. The system can easily be changed to the normal open field configuration and can also be fitted with a minibeam collimator shaping beams of up to 500 μm wide.

To validate physical dosimetry and detect possible bystander effects, biological dosimetry was applied, which allows the detection of radiation effects on a cellular level.[25] The well-established cytokinesis-block micronucleus assay was performed to evaluate micronuclei formation as a biological endpoint[26] resulting from DNA and chromosome damage.

Methods and Materials

Setup of the microbeam source

X-ray source

For the production of microbeams, we integrated a multislit collimator into the Small Animal Radiation Research Platform (SARRP) and the small-animal irradiator XenX (Xstrahl, Camberley, UK). The experiments presented in this article were conducted using the XenX platform located at the XXX. The platform accommodates a Comet MXR-225/22 x-ray tube (Varian Medical Systems, Salt Lake City, UT) installed on a rotating gantry and is equipped with a motorized sample stage. The mean spectral energy of the x-ray tube is approximately 80 keV when operated with filtering of 0.8 mm beryllium and 0.15 mm copper (calculated from a Monte Carlo simulation using the x-ray tube specifications and the mass attenuation coefficients derived from Berger et al[27]). The anode has a target angle of 20 degrees and offers a dual focal spot mode. Experiments were conducted using the small focal spot (0.82 × 0.8 mm^2) at a maximum tube power of 640W and the large focal spot (3.55 × 2.95 mm^2) at 3000W. Varian provides the focal spot sizes according to the norm EN 12543-1.[28]

Microbeam and minibeam collimator

To generate spatially fractionated radiation fields, a custom-made tungsten multislit collimator was developed that shapes the homogeneous radiation field into multiple microbeams at a distance of 212 mm from the x-ray source. It consists of 3 parallel plates and has a total thickness of 7 mm. The collimator comprises 51 slits of 100 µm width and 20 mm height, separated by a center-to-center (ctc) distance of 400 µm on the sample side. The slits are not parallel but are tilted and follow the beam divergence of the x-ray source similar to previous setups.[22] A cross-section of the collimator is shown in Figure 1.

The collimator was manufactured using wire-cutting techniques (T&G Engineering Ltd, West Byfleet, UK). During the manufacturing process, the 3 plates were fixed to each other to guarantee slit alignment. The 3.5-mm-thick middle plate of the collimator was mounted movably between the upper and lower plate, allowing for variable slit width of up to 100 µm.

The described collimator design has 3 main features contributing to improvement of the microbeam field characteristics compared with previous compact sources. First, the tilted slits follow the beam divergence and enhance field homogeneity. Second, the source distance was chosen as a compromise between field homogeneity and low divergence on one hand and a high dose rate on the other hand. Third, the projected focal spot size was made adjustable by a flexible collimator orientation. In addition, the setup provides variable slit widths and hence flexibility for preclinical experiments.

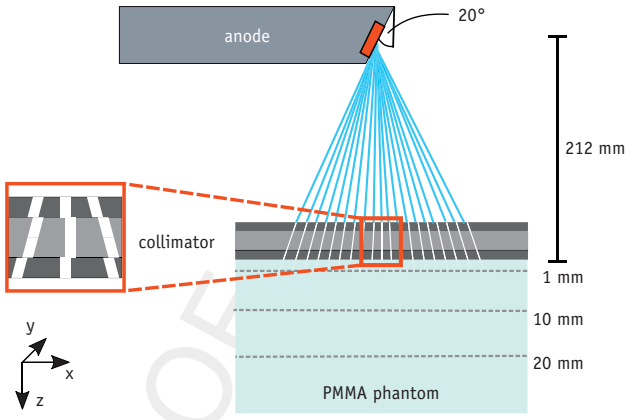

Fig. 1. Schematic view of the microbeam experiment. A conventional x-ray tube with a 20-degree target angle radiates onto a multislit collimator at a 212-mm source distance. The collimator slits are tilted to account for beam divergence, and the collimator middle plate can be shifted to adjust the effective slit width (see magnified view in the red box). Dosimetry is performed in a PMMA phantom with dimensions of 55 × 55 × 100 mm^3 in depths of 1, 10, and 20 mm. (A color version of this figure is available at https://doi.org/10.1016/j.ijrobp.2020.09.039.)

Similarly, a minibeam collimator was manufactured (FEOB Inc, Forstern, Germany) with 11 slits of 500 µm width and 2 mm spacing. The movable middle plate offers slit widths between 0 and 500 µm. Fields are referred to as microbeams if generated with the microbeam collimator and as minibeams if generated with the minibeam collimator.

Integration of the collimator into the experimental setup

The mouse holder provided by the XenX has a source distance of 350 mm and can only take low weight. Therefore, an aluminum frame and a stand were designed to mount the collimator to the motorized sample stage of the XenX as depicted in Figure 2A. The system was set up so that both bottom-up and top-down irradiations could be conducted. Translational positioning of the collimator was carried out using the XenX motorized stage. In addition, the developed setup offered a further degree of freedom for the collimator orientation: By guiding the collimator along a curved recess in the aluminum frame, the angle between collimator and anode could be adjusted (Fig. 2D).

Adjustment of the slit width was accomplished by 2 PIAK10 piezo actuators (Thorlabs Inc, Dachau/Munich, Germany) with a typical step size of 20 nm and a travel range of 10 mm. A connected controller offers external motion control on the computer via the Thorlabs software. The PIAK10 operates only in open-loop mode and lacks a feedback system on the actuator position. Therefore, the sensor GT2-P12K (Keyence, Neu-Isenburg, Germany) was installed as an external feedback system. Using an elastic sensor head and an integrated CMOS sensor with an

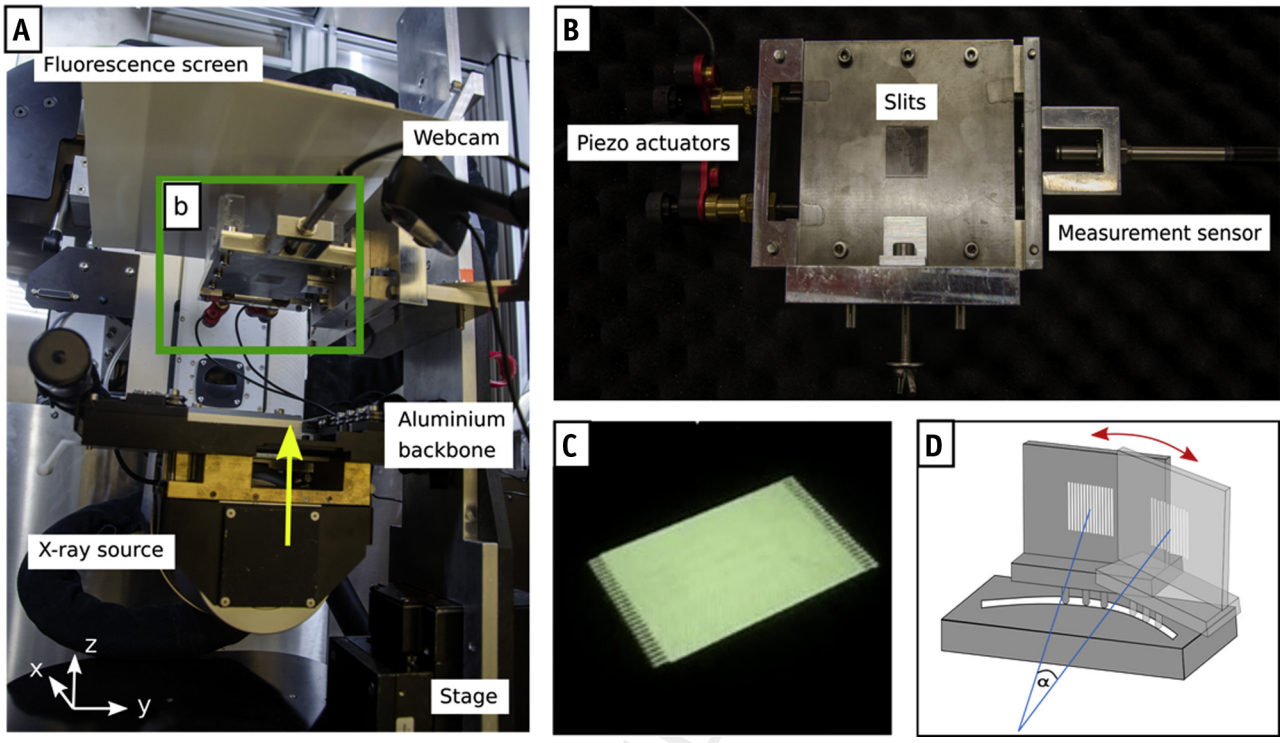

Fig. 2. (A) Photograph of the experimental microbeam setup integrated to the XenX x-ray cabinet. (B) Magnification of the collimator system, including 2 piezo actuators and a measurement sensor for variation of the slit width. (C) The microbeam field monitored by the fluorescence screen. (D) Depiction of how the collimator is guided along the curved recess in the aluminum frame.

absolute scale, it detects position changes with a constant resolution of 1 m over a range of 12 mm.

Both the actuators and the measurement sensor were integrated to the aluminum frame holding the collimator, as shown in Figure 2B, and are not part of the XenX system.

Adjustment procedures

To generate reproducible microbeam fields, the collimator position relative to the anode and the slit width were adjusted before each experiment. In the envisaged experimental starting configuration, the collimator slits were aligned with the anode in x-direction (Fig. 1), and the slits were completely open. This configuration maximizes the radiation intensity behind the collimator with regard to collimator position and slit width. Therefore, it can be determined based on relative intensity measurements.

The microbeam field intensity was qualitatively observed on a fluorescence screen with green light emission (CAWO solutions, Schrobenhausen, Germany) and monitored by a C930 webcam (Logitech, Lausanne, Switzerland) that we mounted to the aluminum frame (Fig. 2A). An example for an observed microbeam field is depicted in Figure 2C. To reduce noise, the intensity was integrated over a time interval of 10 seconds and the entire microbeam field. For gradual variation of either the slit width or the collimator position, the changing intensity was recorded using MATLAB (MathWorks Inc, Natick, MA).

Film dosimetry

For all experiments, the x-ray tube voltage was held constant at 225 kV. Maximum tube currents are 2.8 mA for the small focal spot and 13 mA for the large focal spot. Microbeam experiments were conducted for both focal-spot sizes, whereas minibeam experiments used the large focal spot only. Dosimetry was performed using Gafchromic EBT3 films (Ashland Inc, Covington, KY). EBT3 films provide an optimum dose range between 0.2 and 10 Gy and a spatial resolution of at least 25 μm according to the manufacturer. However, higher resolutions have been achieved experimentally.[22,29] The radiation fields were measured in a 55 × 55 × 100 mm^3 PMMA phantom. For Q7 microbeams, dose was measured in depths of 1, 10, and 20 mm and averaged over 10 mm parallel to the microbeams. For the minibeams, dose was continuously measured over depth with a film oriented perpendicular to the microbeams and parallel to the beam direction. The peak and valley doses were measured separately, and exposure times were selected to keep the absorbed dose between 1 and 6 Gy.

Except for read-out and irradiation, films were wrapped in aluminum foil to protect them from undesired exposure to ambient light. More than 24 hours after irradiation, films were scanned using an optical upright Axio Imager Z1 microscope (Zeiss, Oberkochen, Germany) following Bartzsch et al.[30] Film orientation was kept constant for all

microscope readouts, and scans were performed with white LED light. A monochromatic camera imaged the films through an EC Plan Neofluar objective with 5× magnification and a resolution of 1.29 μm. The Zeiss software AxioVision SE64 recorded stitched images, which were exported to MATLAB. Sample inspections showed no difference between readout with white light and the frequently used red color channel.[31]

Calibration of the films was carried out by exposing a set of films to homogeneous reference doses between 1 and 10 Gy. Reference dosimetry was done using a Farmer TM30010-1 ionization chamber (PTW, Freiburg, Germany) following the TRS398 protocol.[32] The chamber was calibrated by the Physikalische-Technische Bundesanstalt in Braunschweig, Germany, for a 150-kVp x-ray field with a 0.8 mm beryllium and 0.5 mm copper filter. The films and the ionization chamber were irradiated using the same filtering but 220 kV tube voltage. The difference in beam quality was corrected by the beam quality correction factor k_Q.

Finally, the microscope images were converted to dose and averaged over 4 × 4 pixels (5.16 × 5.16 m^2) using MATLAB to compromise between low noise and high resolution of the microbeam structure. Peak dose rate is defined as the mean over the central 20% of the peak width and valley dose rate as the mean over a range of 140 μm in the central valley.

Biological dosimetry

Normal CHO-K1 tissue cells were cultivated in RPMI-1640 growth medium, supplemented with 10% fetal bovine serum, 1% L-glutamine, 1% penicillin-streptomycin, and 1% sodium pyruvate (all from Sigma-Aldrich, Steinheim, Germany). We seeded 6 × 10^4 cells on Nunc Laboratory-Tek II chamber slides with a seeding area of 20 mm × 20 mm. Irradiations were performed with an x-ray tube voltage of 225 kV and a tube current of 13 mA. Microbeams were produced using the microbeam collimator with the large focal spot and a slit width of 50 μm (ctc 400 μm). The chamber slides were placed directly on the collimator surface and were irradiated using the bottom-up configuration of the setup to increase peak dose rate and PVDR. During irradiation, the cells were covered with 2 mL of medium to prevent drying up. Film dosimetry was performed before the cell experiments: small pieces of EBT3 films were placed into a chamber slide and covered by a piece of PMMA having the same filling volume as the medium. Based on the results, the irradiation times of the separate peak and valley irradiations were adjusted such that a peak dose rate of 3.05 Gy/min and a valley dose rate of 0.075 Gy/min were delivered to the cells. Treatment with 3 g/mL cytochalasin B right after irradiation resulted in binuclear cells, which allowed identification of micronuclei exclusively in cells that had undergone only 1 nuclear division after irradiation.[33] Twenty-seven hours after irradiation, the cells were fixed and stained with DAPI. Using Metafer (Metasystems, Altlussheim, Germany) at an automated fluorescence microscope Axio Observer 7 (Zeiss, Oberkochen, Germany), the micronuclei and binuclear cells were automatically analyzed and the exact coordinates of the cells determined. A reference curve was established using homogeneous irradiation with doses from 0 to 4 Gy and a dose rate of 7.2 Gy/min. At least 1000 cells per dose were counted. To get spatial information, the position of cells relative to the next microbeam center was scored in bins of 12.5-μm and 25-μm widths for peak and valley irradiations, respectively.

Monte Carlo simulations

Monte Carlo simulations were carried out in the 10.4.2 version of Geant4 software using the low-energy Penelope physics library. The dimensions of the tungsten collimator and the geometry of the setup followed the technical design of the experiment. The focal spot of the anode was modeled by a Gaussian distribution based on focal spot dimensions provided by the manufacturer and with an energy distribution according to the simulated x-ray tube spectrum. We simulated 10^9 photon histories, and primary and secondary particles were tracked with a cut-off range of 1 μm. The energy deposited in the PMMA phantom is scored along a cartesian grid with voxel sizes of 5 m × 100 m × 1 mm ($x \times y \times z$; Fig. 1).

Comparisons between open-field dose measurements and corresponding simulations were used to calibrate the scored energy to dose rate. In addition, reference measurements with the XenX were conducted to verify the focal spot model. To validate the model of the x-ray source, a pinhole aperture of 500 μm diameter was mounted onto a brass collimation nozzle 18.5 cm long (both provided by Xstrahl), and the focal spot was projected onto an EBT3 film at a source distance of 35.5 cm. The geometry was mimicked in Monte Carlo, and simulated dose profiles were compared with the film measurements.

Results

Setup of the microbeam source

The horizontal position of the collimator along the x-axis (Fig. 1) was determined with an accuracy of at least 100 μm using the fluorescent screen, the webcam, and MATLAB intensity analysis. Figure 3 shows the underlying relation between the total intensity of all beams and the horizontal position of the collimator. At the position of maximum output, the tilted collimator slits focused on the x-ray source. With increasing distance from this position, the slits lost focus and the intensity output rapidly decreased. The intensity was less sensitive to the alignment along the y-axis and z-axis. Therefore, y and z positions were measured a single time and kept constant for all experiments.

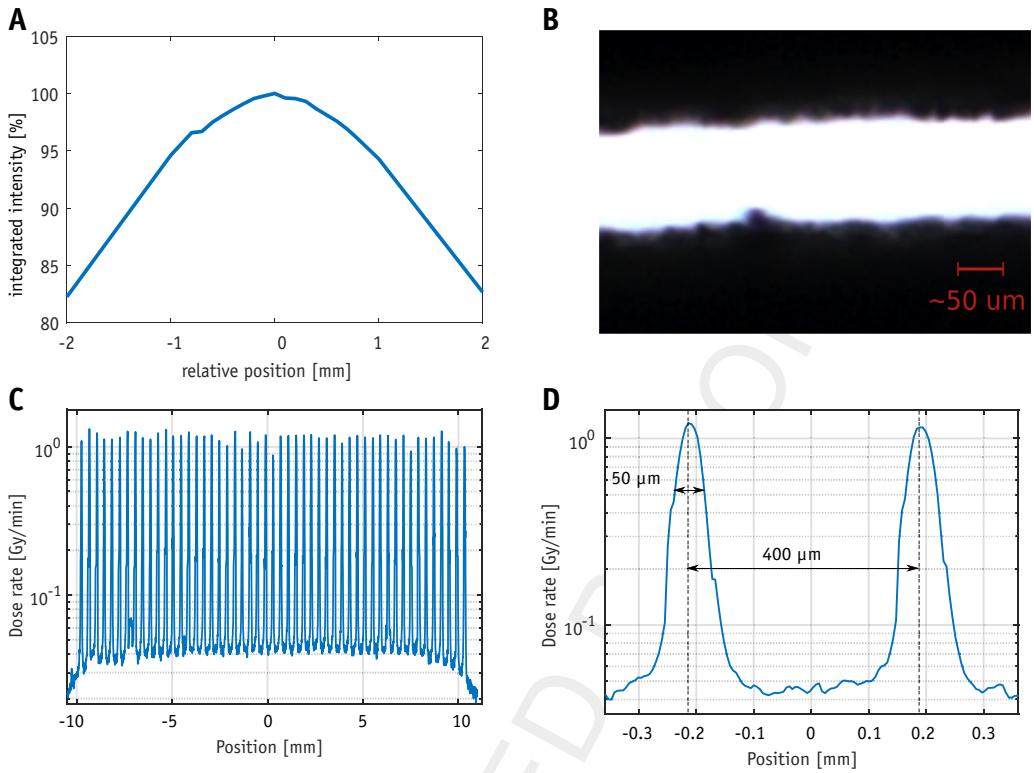

Fig. 3. (A) Relation between the integrated intensity of all beams and the horizontal collimator position. The intensity is normalized to its maximum. (B) Magnified microscopic image revealing the rough surfaces of a fully opened microbeam collimator slit. (C, D) The film dosimetry profile of a microbeam field with beams 50 µm wide was obtained by combining 2 independent measurements with either peak or valley dose in the range between 1 and 6 Gy.

The initial slit width of 100 µm was adjusted with a tolerance of 1 µm. The impact of this deviation was evaluated by Monte Carlo simulations, which showed that the related uncertainties of peak dose rate and PVDR were less than 5% for beams 50 µm wide.

Film dosimetry

Microbeam field characteristics

Figure 3 shows the microbeam profiles measured for a slit width of 50 µm at 1 mm depth in the phantom. The profiles represent the dose average over 2.58 mm parallel to the beams in the center of the microbeam field.

Peak doses are characterized by high uniformity with a relative mean absolute deviation of the median peak dose rate across the profile of 5% (Fig. 3). This deviation increased with increasing depth in phantom and decreasing slit width. For a slit width of 25 µm, the peak dose rate across the profile varied by 15% around the median in 20 mm depth. In contrast, the valley dose rate followed a pillow-shaped curve with an approximately symmetrical decrease toward the edges. Figure 3 shows details of the profile and demonstrates the well-resolved microbeam structure on the EBT3 films.

The full width at half maximum of the peaks was measured in dependence of the adjusted beam width in 1 mm distance from the collimator. Mean peak widths of 103 µm and 48 µm were achieved for intended values of 100 µm and 50 µm. With a measured value of 35 µm, the deviation was larger for an aimed peak width of 25 µm. Beam widths varied across the profile, with a relative standard deviation between 7% and 10%. The variation can be explained by manufacturing inaccuracies and rough collimator surfaces, as shown in Figure 3.

A series of 4 independent measurements including calibration of the setup, irradiation, microscopy, and analysis for slit widths of 100 µm and 50 µm proved high reproducibility of the peak dose rate and the peak width within an uncertainty of 5% and 4%, respectively. Scans of the film with the microscope and analysis could be reproduced with a relative standard deviation less than 3.5% in a series of 3 measurements.

The main results of microbeam film dosimetry are summarized in Table 1 and analyzed in the following section.

Impact of the collimator slit width

Measurements at depths of 1, 10, and 20 mm assessed the influence of the collimator slit width on microbeam peak dose rate, valley dose rate, and PVDR and are visualized in Figure 4. All data points represent the median values across the profile. The error bars consider the mean absolute

Table 1 Results from microbeam film dosimetry for different depths in phantom, slit widths, focal spot sizes, and target angles*

Depth, mm	1	10	20	10	10	10	10	1	10
Beam width, μm	50	**50**	50	25	100	50	50	50	50
Focal spot	Fine	**Fine**	Fine	Fine	Fine	Broad	Fine	Broad	Broad
Target angle, degrees	20	**20**	20	20	20	20	12	12	12
Peak dose rate, Gy/min	1.17	**0.83**	0.56	0.63	1.13	2.71	1.09	8.0	4.6
Valley dose rate, Gy/min	0.042	**0.046**	0.044	0.030	0.085	0.21	0.044	0.205	0.25
PVDR	28	**18**	13	21	13	13	25	39	18

Abbreviation: PVDR = peak-to-valley dose ratio.

* The reference measurement was conducted in a depth of 10 mm for a slit width of 50 μm, the small focal spot ($0.82 \times 0.8 mm^2$), and the default target angle of 20 degrees. For the remaining measurements, 1 parameter was varied, respectively, and all others remained constant. All measurements were conducted using the microbeam collimator. PVDRs are rounded to integer values.

deviation across the profile, the uniformity of EBT3 films of 3%, uncertainties from the dose calibration, and an error of 2% accounting for the absolute dose measurement with the ionization chamber.

Smaller slit width led to a reduced dose rate in the peak and also to a reduction of valley dose rates owing to less scattering. The ratio between ctc and slit width is particularly important for the PVDR: If this ratio increases, the scatter dose in the valley decreases, and hence, the PVDR becomes higher.

With depth in the phantom, the peak dose rate decreased as a consequence of attenuation and scattering. Close to the beam entrance, a substantial fraction of photons scatter out of the phantom, and therefore, the valley dose rate increases within the first few millimeters in depth. The valley dose rate reaches a plateau at a depth of about 10 mm and starts to decline together with the peak dose rate. However, in contrast with synchrotron-generated microbeams, the PVDR does not become constant in depth but is steadily decreasing because of the beam divergence.

Impact of the focal spot size

Figures 5B and 5E compare the 2 focal spot sizes provided by the XenX x-ray tube in terms of microbeam peak dose

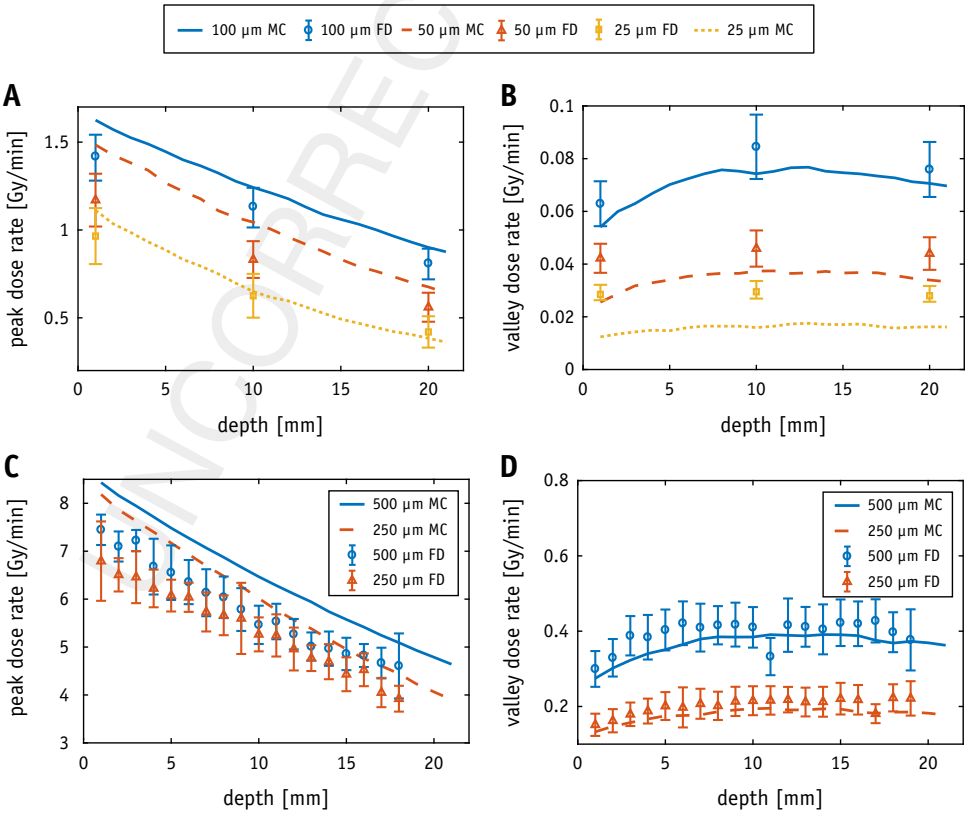

Fig. 4. Impact of the collimator slit width on the measured peak dose rate (A, C) and valley dose rate (B, D) in different phantom depths. The results of film dosimetry and Monte Carlo simulations are compared for microbeams (A, B) and minibeams (C, D).

rate and PVDR. Both experiments were conducted with the microbeam collimator and a slit width of 50 μm. Although the large focal spot (3.55 × 2.95 mm^2) was used with the maximum tube current of up to 13 mA, the small focal spot (0.82 × 0.8 mm^2) was limited to a maximum current of 2.8 mA. At a depth of 1 mm, the ratio of the peak dose rate between the 2 focal spots was approximately 4.6 and reflected the ratio between the tube currents. With increasing depth, the peak dose rate of the large focal spot decreased more rapidly compared with the small focal spot because of larger beam penumbras and the related degradation of the microbeam structure. For the same reason, the decrease of the PVDR with depth is less steep for the small focal spot than for the large focal spot. Quantitatively, the PVDR was improved by up to 125% in a depth of 20 mm when using the small focal spot.

Impact of the target angle

Figure 5G illustrates the reduction of the effective focal spot size with the angle between collimator and anode, here termed *target angle*. In the experiment, the microbeam collimator was rotated around the anode to reduce the default target angle of 20 degrees to the smallest possible value of 10 degrees.

Reducing the target angle improved both peak dose rate and PVDR by up to 39% as demonstrated in Figures 5A and 5D.

Comparison of microbeams and minibeams

Figure 4 compares film dosimetry and simulations of microbeam fields to minibeam fields with slit widths of 500 μm and 250 μm. Benefitting from the large slit widths and the use of the large focal spot, the minibeam system reached peak dose rates of 7.6 Gy/min, whereas the peak dose rates of the microbeam system with the small focal spot were less than 1.5 Gy/min. However, using the combination of the large focal spot and the decreased target angle of 12 degrees increased the microbeam peak dose rates to up to 8 Gy/min. The decrease of peak dose rate and valley dose rate over depth showed a similar tendency for both minibeams and microbeams. Furthermore, the impact of the minibeam slit width on the dose rate was comparable to the impact of the slit width for microbeams (100 μm and 50 μm). In Figure 5H, the PVDR measured for minibeams and microbeams in depths of 1 and 10 mm are summarized. PVDRs of minibeams and microbeams at equal ratios of ctc and slit width are expected to be similar.

Comparison between experiment and simulation

For validation of the experiment, the results were compared with Monte Carlo calculations. Monte Carlo results were calibrated in open-field geometry to provide quantitative results. The reference measurements of the pinhole focal-spot projection agreed with the simulation within the measurement uncertainties. Minor deviations of less than 10% were observed only at the edge of the focal spot. The impact of these deviations on the microbeam peak dose and PVDR was estimated to be less than 5% in a depth of up to 20 mm.

The results from the microbeam experiments were compared in depths of 1, 10, and 20 mm. The microbeam peak dose rates from Monte Carlo were 10% to 27% higher than the results from film dosimetry. The valley dose rates were between 7% and 56% lower. As a result, owing to the uncertainties in both the peak and the valley dose rates, the simulation predicted much higher values for the PVDR than observed in the experiment. These deviations were observed to increase with smaller slit widths and evidenced the challenging beam production and detection mechanisms for beams of small width.

For minibeams, the deviations in the simulated peak dose rate from the experiment were between 10% and 20%. The simulated valley dose rate deviated up to 20% from the experiment except for 2 values within the measurement uncertainties. Minibeam simulations showed better agreement with measurements than microbeam simulations, as expected from the larger slit widths (Fig. 4). Monte Carlo simulations predict approximately 20% higher minibeam peak dose rates than shown in the measurements, most likely because of unaccounted scattering at uneven collimator surfaces.

Although the experiment and simulation deviated in absolute numbers, the qualitative agreement is good. In particular, the experimentally observed dependence of dose on depth and the collimator slit width is well reflected by the simulation results.

Biological dosimetry

Cell exposure with homogeneous fields was used to create a reference curve for biological dosimetry. The dose response curve shows a linear increase of micronuclei per binucleated cell (MN/BN). Accurate measurements were possible only for doses from 0.1 Gy up to 4 Gy. For the microbeam dose profiles in Figure 5, the micronucleus yield of all cells within the same bin were averaged. A peak dose of 2 Gy (film dosimetry) results in a mean micronucleus yield of 1.05 ± 0.05 MN/BN in the peaks, corresponding to 2.13 ± 0.11 Gy (biological dosimetry). However, irradiations with a calculated valley dose of 2 Gy result in a slightly higher mean micronucleus yield of 1.08 ± 0.04 MN/BN in the valleys, which equals 2.35 ± 0.10 Gy (Fig. 5F).

Discussion

We presented a method to produce microbeams and minibeams in the small-animal irradiators SARRP and XenX, which can be used for in vitro and in vivo preclinical research. A microbeam and a minibeam collimator provide beam spacing of 400 mm and 2 mm with beam width of up to 100 μm and 500 μm, respectively. The set-up allows flexibility in the choice of beam width by use of a 3-layered

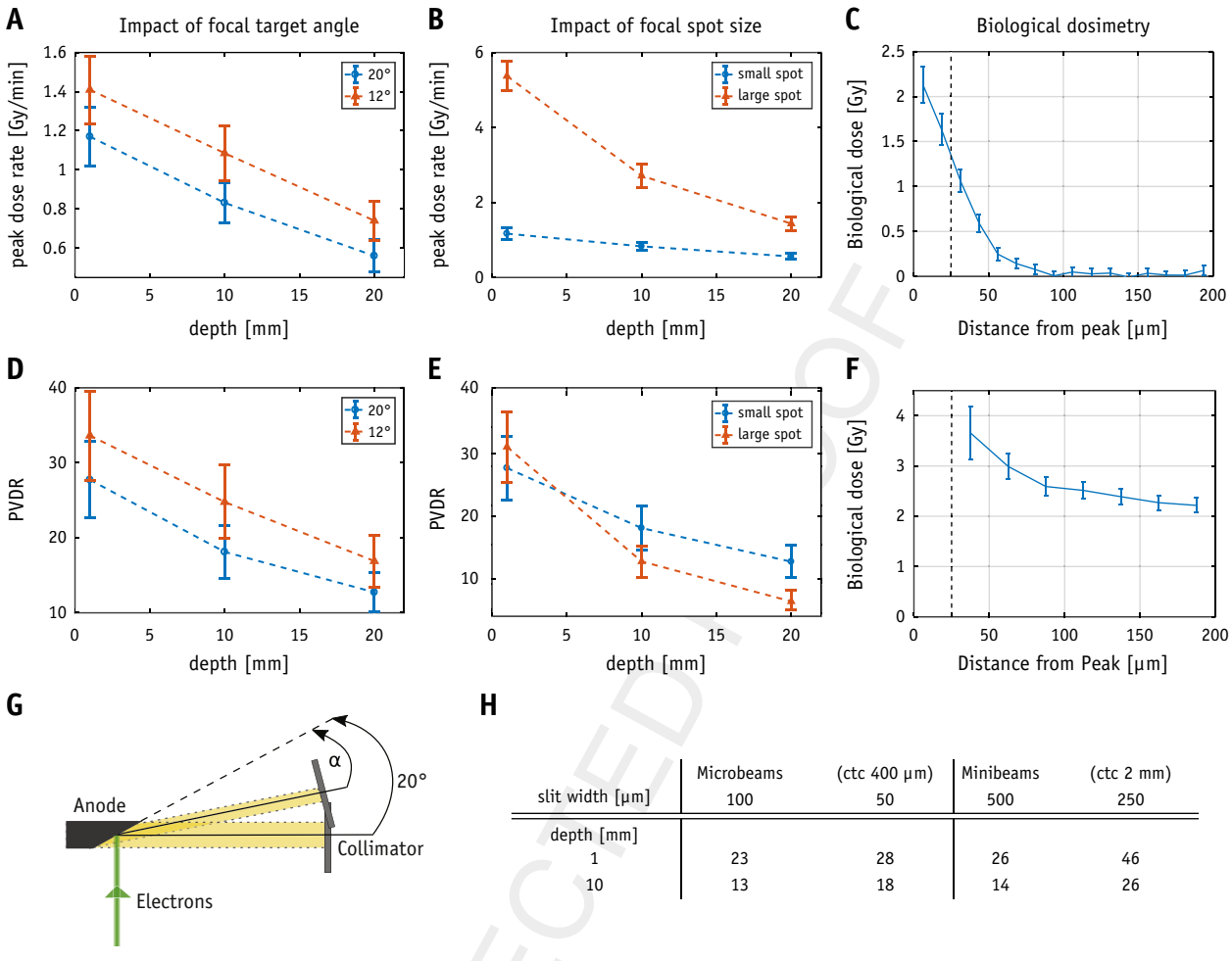

slit width [µm]	Microbeams 100	(ctc 400 µm) 50	Minibeams 500	(ctc 2 mm) 250
depth [mm]				
1	23	28	26	46
10	13	18	14	26

Fig. 5. The left column illustrates the impact of the target angle on peak dose rate (A) and peak-to-valley dose ratio (PVDR) (D) in the microbeam fields. The schematic drawing in G shows the change of the target angle in the experimental setup. The central column shows the impact of the focal spot size on the measured microbeam peak dose rate (B) and PVDR (E) in different phantom depths. Small and large focal spots have dimensions of 0.82 × 0.8mm^2 and 3.55 × 2.95mm^2, respectively. Biological dosimetry profiles using micronuclei are shown for a peak dose of 2 Gy (C) and a valley dose of 2 Gy (F). The table (H) summarizes PVDRs measured for minibeams and microbeams using the large and small focal spot, respectively.

collimator design. Calibration procedures ensure reproducibility of the generated radiation fields. Various measures were taken to improve the field properties compared with designs in the past, resulting in the first time microbeam widths less than 100 µm have been used for preclinical in vivo experiments at reasonable dose rates and field properties.

The generated microbeams were characterized with film dosimetry and benchmarked to Monte Carlo simulations. In the past, microbeams with 50 µm width and 400 µm spacing were considered a good compromise between tumor control and normal tissue sparing.[34] The PVDR of a 20 mm × 20 mm radiation field of such microbeams is greater than 18 within the first centimeter in a PMMA phantom. The PVDR of minibeams with the same ratio of spacing and beam width (ie, a beam width of 250 µm and a beam spacing of 2000 µm) leads to even higher PVDRs of greater than 25. Such PVDRs are similar to those achieved with synchrotron-generated microbeams[30,35] and higher than for most other x-ray tube–based minibeam or microbeam systems.[20,24] In contrast to synchrotrons, the PVDR at the presented setup strongly decreased with depth, but nevertheless, the decrease was sufficiently shallow to treat mice when positioned close to the collimator surface.

Compared with a former microbeam setup[22] and former setups with small-animal radiation systems,[20,24] the field homogeneity in terms of peak dose rates was substantially improved to standard deviations of 5% to 8% and is similarly low compared with reported values for synchrotron generated microbeams.[36]

Whereas peak entrance dose rates at the synchrotron for MRT are up to 10 kGy/s, the presented setup achieves only up to 8.0 Gy/min for microbeams, depending on the choice of the focal spot and beam width. Such low dose rates

require an immobilization of the target to avoid dose blurring owing to organ motion. However, considering that mice can be anaesthetized safely for up to 1 hour, MRT typical peak doses of approximately 400 Gy can be applied.

Similar to Esplen et al,[24] we found that using the small focal spot size improves the PVDR but reduces the dose rate because of the reduced maximum tube power. Therefore, the larger focal spot size seems beneficial for use in small-animal experiments. A way to further improve both PVDR and peak dose rate is pivoting the collimator relative to the x-ray tube and thus reducing the beam emission angle. Dosimetry results show that a reduction of the emission angle from 20 degrees to 12 degrees leads to an increase in PVDR of up to 39% and in peak dose rate of up to 31% in a depth of 10 mm with the small focal spot. The combination of the decreased emission angle and the broad focal spot leads to a similar increase of 38% for the PVDR and an even higher increase in peak dose rate of 70%. This configuration leads to the stated maximum peak dose rate of 8 Gy/min and is therefore considered favorable for small-animal experiments. The described findings from our experiments are expected to be transferable to other small-animal irradiators.

Comparisons to Monte Carlo simulations reveal good qualitative agreement, but considerable quantitative differences are observed between measured and simulated doses. Particularly at small beam widths, differences between measurement and simulation can be up to 100%. We suspect the reasons for these differences are rough collimator surfaces, fabrication tolerances, and dust between the collimator slits, which could not have been modeled and become important at smaller slit widths. These confounders will most likely reduce the peak dose rate and increase the scattering into the valley as observed in this study's results. The strong deviations between simulation and measurement illustrate the challenging fabrication process of collimators with micrometer-sized apertures. For treatment planning, a parameterized Monte Carlo model is currently being developed that accounts for the discrepancies between ideal and realistic setups in a parameterized model. Apart from that, the model of the x-ray−source phase space may not be accurate enough. Because focal-spot and collimator-slit apertures are of similar width, the dose in the microbeam field sensitively depends on the precise shape of the focal spot.

The detected biological damage in the peaks was mostly in accordance with the film dosimetry. For the valley irradiations, slightly higher doses were observed, which could have been caused by possible bystander effects.

Conclusion

This study presented a method to produce microbeams and minibeams with flexible widths of up to 100 μm and 500 μm and peak dose rates of up to 8 Gy/min at the small-animal irradiators XenX and SARRP from Xstrahl. Peak and valley dose rates, field homogeneity, and the beam penumbras were characterized in measurements and Monte Carlo simulations. It was shown that a reduction of the beam emission angle improves PVDR and dose rate. The choice of a small focal spot increases the PVDR and beam shape but reduces the dose rate. The combination of a small beam-emission angle and a large focal spot provides a good compromise between high PVDR and high peak dose rates. The developed setup produces microbeam fields with suitable properties for in vivo experiments with mice and meets the high technical requirements to enable preclinical MRT in commercially available small-animal irradiators.

References

1. Bartzsch S, Corde S, Crosbie JC, et al. Technical advances in x-ray microbeam radiation therapy. *Phys Med Biol* 2020;65:02TR01.
2. Bräuer-Krisch E, Serduc R, Siegbahn EA, et al. Effects of pulsed, spatially fractionated, microscopic synchrotron X-ray beams on normal and tumoral brain tissue. *Mutat Res* 2010;704:160-166.
3. Bouchet A, Lemasson B, Le Duc G, et al. Preferential effect of synchrotron microbeam radiation therapy on intracerebral 9l gliosarcoma vascular networks. *Int J Radiat Oncol Biol Phys* 2010;78:1503-1512.
4. Laissue JA, Blattmann H, Di Michiel M, et al. Weanling piglet cerebellum: A surrogate for tolerance to MRT (microbeam radiation therapy) in pediatric neuro-oncology. *Proc SPIE* 2001;4508:65-73.
5. Serduc R, van de Looij Y, Francony G, et al. Characterization and quantification of cerebral edema induced by synchrotron x-ray microbeam radiation therapy. *Phys Med Biol* 2008;53:1153.
6. Slatkin DN, Spanne P, Dilmanian FA, Gebbers J-O, Laissue JA. Subacute neuropathological effects of microplanar beams of x-rays from a synchrotron wiggler. *Proc Natl Acad Sci U S A* 1995;92:8783-8787.
7. Laissue JA, Geiser G, Spanne PO, et al. Neuropathology of ablation of rat gliosarcomas and contiguous brain tissues using a microplanar beam of synchrotron-wigglergenerated x rays. *Int J Canc* 1998;78:654-660.
8. Miura M, Blattmann H, Bräuer-Krisch E, et al. Radiosurgical palliation of aggressive murine sccvii squamous cell carcinomas using synchrotron-generated x-ray microbeams. *Br J Radiol* 2006;79:71-75.
9. Bouchet A, Bräuer-Krisch E, Prezado Y, et al. Better efficacy of synchrotron spatially microfractionated radiation therapy than uniform radiation therapy on glioma. *Int J Radiat Oncol Biol Phys* 2016;95:1485-1494.
10. Ibahim MJ, Yang Y, Crosbie JC, et al. Eosinophil-associated gene pathways but not eosinophil numbers are differentially regulated between synchrotron microbeam radiation treatment and synchrotron broad-beam treatment by 48 hours postirradiation. *Radiat Res* 2015;185:60-68.
11. Bouchet A, Sakakini N, El Atifi M, et al. Early gene expression analysis in 9l orthotopic tumor-bearing rats identifies immune modulation in molecular response to synchrotron microbeam radiation therapy. *PLoS One* 2013;8:e81874.
12. de Sola FM, Vilches M, Prezado Y, Lallena AM. Impact of cardiosynchronous brain pulsations on Monte Carlo calculated doses for synchrotron micro-and minibeam radiation therapy. *Med Phys* 2018;45:3379-3390.
13. Donzelli M, Bräuer-Krisch E, Oelfke U. Brain motion induced artefacts in microbeam radiation therapy: A Monte Carlo study. *Radiother Oncol* 2016;118:S34-S35.

14. Jacquet M, Suortti P. Radiation therapy at compact Compton sources. *Phys Med* 2015;31:596-600.
15. Burger K, Ilicic K, Dierolf M, et al. Increased cell survival and cytogenetic integrity by spatial dose redistribution at a compact synchrotron x-ray source. *PLoS One* 2017;12:e0186005.
16. Schreiber EC, Chang SX. Monte Carlo simulation of a compact microbeam radiotherapy system based on carbon nanotube field emission technology. *Med Phys* 2012;39:4669-4678.
17. Bartzsch S, Oelfke U. Line focus x-ray tubes—a new concept to produce high brilliance x-rays. *Phys Med Biol* 2017;62:8600.
18. Babcock K, Sidhu N, Kundapur V, Ali K. Collimator design for experimental minibeam radiation therapy. *Med Phys* 2011;38:2192-2197.
19. Bazyar S, Inscoe CR, O'Brian ET, Zhou O, Lee YZ. Minibeam radiotherapy with small animal irradiators: In vitro and in vivo feasibility studies. *Phys Med Biol* 2017;62:8924.
20. Prezado Y, Dos Santos M, Gonzalez W, et al. Transfer of minibeam radiation therapy into a cost-effective equipment for radiobiological studies: a proof of concept. *Sci Rep* 2017;7:17295.
21. Zhang L, Yuan H, Burk LM, et al. Image-guided microbeam irradiation to brain tumour bearing mice using a carbon nanotube x-ray source array. *Phys Med Biol* 2014;59:1283.
22. Bartzsch S, Cummings C, Eismann S, Oelfke U. A preclinical microbeam facility with a conventional x-ray tube. *Med Phys* 2016;43:6301-6308.
23. Wong J, Armour E, Kazanzides P, et al. High-resolution, small animal radiation research platform with x-ray tomographic guidance capabilities. *Int J Radiat Oncol Biol Phys* 2008;71:1591-1599.
24. Esplen NM, Chergui L, Johnstone CD, Bazalova-Carter M. Monte Carlo optimization of a microbeam collimator design for use on the small animal radiation research platform (SARRP). *Phys Med Biol* 2018;63:175004.
25. Bundesamt für Strahlenschutz. Biological Dosimetry Following Radiation Exposure. Available at: https://www.bfs.de/EN/topics/ion/service/dosimetry/biological-dosimetry/biological-dosimetry.html. Accessed. Q9
26. Luzhna L, Kathiria P, Kovalchuk O. Micronuclei in genotoxicity assessment: From genetics to epigenetics and beyond. *Front Genet* 2013;4:131.
27. Berger M, Hubbel J, Steltzer S, et al. Xcom: Photon cross section database. National Institute of Standards and Technology, version 3.1; 2010. Available at: https://www.nist.gov/pml/xcom-photon-cross-sections-database. Accessed January 2020. Q10
28. German Institute for Standardisation. Non-Destructive Testing: Characteristics of Focal Spots in Industrial X-Ray Systems for Use in Non-Destructive Testing —Part 1. Scanning Method. 1999. Q11
29. Burger K. Microbeam radiation therapy at a compact synchrotron x-ray source. Technische Universität München. Available at: https://mediatum.ub.tum.de/doc/1399928/1399928.pdf. Accessed. Q12
30. Bartzsch S, Lott J, Welsch K, Bräuer-Krisch E, Oelfke U. Micrometer-resolved film dosimetry using a microscope in microbeam radiation therapy. *Med Phys* 2015;42:4069-4079.
31. Pellicioli P, Bartzsch S, Donzelli M, Krisch M, Bräuer-Krisch E. High resolution radiochromic film dosimetry: Comparison of a microdensitometer and an optical microscope. *Phys Med* 2019;65:106-113.
32. Andreo P, Burns DT, Hohlfeld K, et al. Absorbed dose determination in external beam radiotherapy. Technical Report 398. Vienna, Austria: International Atomic Energy Agency; 2000.
33. Rodrigues MA, Beaton-Green LA, Wilkins RC, Fenech MF. The potential for complete automated scoring of the cytokinesis block micronucleus cytome assay using imaging flow cytometry. *Mutat Res Genet Toxicol Environ Mutagen* 2018;836:53-64.
34. Serduc R, Bouchet A, Bräuer-Krisch E, et al. Synchrotron microbeam radiation therapy for rat brain tumor palliation—influence of the microbeam width at constant valley dose. *Phys Med Biol* 2009;54:6711.
35. Martínez-Rovira I, Sempau J, Prezado Y. Development and commissioning of a Monte Carlo photon beam model for the forthcoming clinical trials in microbeam radiation therapy. *Med Phys* 2012;39:119-131.
36. Lerch MLF, Petasecca M, Cullen A, et al. Dosimetry of intensive synchrotron microbeams. *Radiat Meas* 2011;46:1560-1565.